T. Magn. Soc. Jpn. (Special Issues)., **3**, 113-119 (2019)

<Paper>

Effect of Ionic Concentration on Dynamic Magnetic Susceptibility of Iron Oxide Nanoparticles Embedded in Chitosan Hydrogel Matrix

M. E. Villamin, and Y. Kitamoto

Tokyo Institute of Technology, Department of Materials Science and Engineering, *4259 Nagatsutacho, Midori-ku, Yokohama, Kanagawa, 226-8502*

We investigate the effect of the ionic strength of surrounding NaCl solutions of an iron-oxide chitosan hydrogel (FeO_x-CH) on magnetic relaxation of the FeO_x NPs. The magnetic relaxation of the FeO_x NPs is examined using dynamic magnetic susceptibility measurement. Swelling ratio (SR) is also measured after the FeO_x-CH is immersed to various NaCl concentrations. SR of the FeO_x-CH decreases as the NaCl concentration increases. This trend is explained by considering the osmotic water flow in the FeO_x-CH. The peak in frequency dependence of the imaginary part of the susceptibility (χ'') is found around 200 Hz. In addition, the position of the χ'' peak frequency shifts to lower frequencies as the NaCl concentration increases. The observed frequency shift is inferred to be due to the suppression of the Brownian relaxation caused by the decrease of SR of the FeO_x-CH as the NaCl concentrations increases. An effective viscosity change of 6.8% due to the change in the NaCl concentration is also estimated via analytical calculation.

Key words: biomagnetism, magnetic nanoparticles, magnetic biosensing, chitosan ferrogel, dynamic susceptibility,

1. Introduction

There is great research interest on the integration of nanostructures with stimuli-responsive polymers for the development of multifunctional materials. One of these multifunctional materials is a ferrogel that exhibits dual-responsiveness to both chemical and magnetic external stimuli [1)-2)]. Such ferrogels are composed of magnetic nanoparticles crosslinked (either via physical or chemical crosslinking) with a stimuli-responsive polymer network. Due to the dual-responsiveness to pH/magnetic or thermal/magnetic, these ferrogels are extensively studied for many biomedical applications for stress sensors [3)], controlled-release of drug [4)], and externally control microfluidics [5)].

In particular, ferrogels are very useful for biosensing applications. In a previous study, we have demonstrated magnetic based pH-detection using an iron oxide – chitosan (FeO_x-CH) ferrogel [6)]. This is achieved by coupling the chemical-responsiveness (pH-sensitivity) of the CH matrix to magnetic relaxation property of the FeO_x nanoparticles (NPs). That is a change in the pH (chemical stimulus) would cause a corresponding change in the magnetic relaxation property of the embedded FeOx NPs, which can then be measured by dynamic magnetic susceptibility. This potentially paves the way for non-contact magnetic-based chemical (pH) sensors based on ferrogels. Note that different polymers may be used to detect different chemical stimuli [7)-10)]. Hence, ferrogel based biosensors are not limited to pH detection.

Potentially, ferrogel-based biosensors can be applied to microarrays. Microarrays are used for simultaneous analyses of different target molecules, such as in DNA microarrays and in protein-based microarrays in a single experiment run. In a conventional microarray, sensing sites that have a unique target molecules are arranged in an array or matrix. The surface of the sensing sites is functionalized so that the target molecules (and only the target molecules) bind to the sites. The bound target molecules are then detected by labeling methods such the use of fluorescent labels or isotopic labels, or non-labeling methods such as mass spectrometry or micro-cantilevers [11)-12)]. In commercially available microarrays, the fluorescent labeling detection method is dominant because of its high throughput and low cost [11)]. However, fluorescent labels often chemically react to target molecules that could potentially alter their intrinsic property [3)] and also sufficient time is required for the reaction to complete. These affect the reliability of the signal detection, and prevent the real-time detection of binding events [11)-13)]. Alternative non-label methods, on the other hand, are still under development.

Clearly, one possible alternative label-free method is the use of a ferrogel based microarray, which utilizes ferrogel sites instead of the functionalized surfaces. The use of magnetic sensing offers potentially label-free, non-contact measurement at possibly real-time detection speeds by using ferrogels. By choosing the appropriate gel matrix material, target molecules could interact directly to the gel without the need for further functionalization. Furthermore, gels also potentially allow to increase the sensing part by using the whole volume of the ferrogel instead of using two-dimensional binding surface.

As mentioned, magnetic based pH sensing has already been previously demonstrated in FeO_x-CH, where changes in pH affected the magnetic relaxation of the NPs, which was then detected by dynamic susceptibility measurements [6)]. As pH changed from pH 1.95 (acidic) to pH 6 (neutral), the peak in the frequency dependent imaginary part of the susceptibility shifted to lower frequency, from ~190 to ~170 Hz [6)]. This is accompanied by a reduction in the swelling ratio (SR) of ferrogel (i.e. the ferrogel reduced swelling and became

smaller). We attributed the shift in the peak of the imaginary part susceptibility to lower frequency due to the change of Brownian relaxation time resulting from the reduced swelling of the CH. This can be interpreted as a change in effective viscosity of CH. The viscosity of the CH changed with pH due to the presence of NH^{2+} vs. NH^{3+} causing the CH to decrease swelling in low pH. This mechanism will be explained in more detail in a latter section.

In this study, we utilize the same material system and demonstrate magnetic-based ionic strength detection. Similar to the previous study, the materials used in this study are the following: CH as the stimuli-responsive polymer, and FeO_x NPs as the superparamagnetic nanoparticles. We note that CH is chemically responsive not only to pH [14)-16),21)] but also to multiple chemicals, including ions (ionic strength sensitivity) [15),17),18),20),22)] and temperature [21)]. Other advantages of using CH are its abundance [22)-23)], biocompatibility [14) - 22)] and ease of functionalization [14), 21)]. Hence, these make CH an ideal candidate for ferrogel biosensors. Whereas, the merits of using FeO_x NPs are biocompatibility [24)], strong magnetic property [24)-26)] and low toxicity [24)], which makes them appropriate for many biomedical applications. Here, we investigated the effect of the change in the ionic strength of the surrounding solution to the magnetic susceptibility of the FeO_x-CH ferrogel, as measured by dynamic magnetic susceptibility.

2. Experimental Details

2.1 Synthesis and characterization of FeOx-CH

The chemicals used in the experiment are as follows: iron(III) chloride hexahydrate ($FeCl_3 \cdot 6H_2O$) and iron(II) chloride tetrahydrate ($FeCl_2 \cdot 4H_2O$) with 99.0 % purity were bought from Wako Pure Chemical Industries, and chitosan powder with ~20000 – 50000 molecular weight, was obtained from the Sigma Aldrich Company.

The synthesis process has been described in detail in a previous study [6)]. For convenience, here we describe the process briefly. First, $FeCl_3.6H_20$ and $FeCl_2.4H_20$ powder (Fe^{3+}/Fe^{2+} ratio of 1/2) were added to a chitosan solution using a magnetic stirrer. Next, the Fe^{3+}/Fe^{2+}/CH aqueous solution was placed in an NH_4OH coagulation bath until the gelation is completed. Lastly, the resulting iron-oxide chitosan hydrogel (FeO_x-CH), which has a distinctive black color, was washed several times with purified water. By measuring the height of the gel formed as function of time, we are able to estimate the gel formation rate. Note that the FeO_x NPs were not functionalized before embedding into the gel. Thus, we assume that the nanoparticles are weakly bound to the chitosan matrix; there is also a possibility that some FeO_x NPs are freely moving or completely not bound to the chitosan matrix.

The final structure of the FeO_x-CH specimens was confirmed by scanning electron microscopy (SEM). Prior to SEM observations, the specimens were coated with osmium. Moreover, the ferrogel formation and FTIR results are also presented.

2.2 Swelling ratio

Swelling ratio (SR) is generally used to evaluate the amount of water absorption of hydrogels. SR values of FeO_x-CH are calculated using equation (1) [27)].

$$SR\ \% = [(W_s - W_d) / W_d] \times 100\%, \quad (1)$$

where W_s is the specimen's weight when swollen after submerging to the solution, and W_d is the specimen's weight after freeze drying for two hours. The sample was immersed in the solution with different NaCl concentrations (10 mM, 100 mM and 500 mM) prior to SR measurements. Note that the sample was washed after each measurement, and then, the same sample was used in the next measurements.

2.3 Dynamic Magnetic Susceptibility Measurement

For the magnetic characterization, we measured dynamic magnetic susceptibility (sometimes referred to as the AC susceptibility or frequency dependent susceptibility) under alternating fields of the FeO_x-CH using a Physical Property Measurement System (Quantum Design Corp.: PPMS). The dynamic susceptibility represents dynamic magnetic responses of the FeO_x NPs inside the CH. Susceptibility is simply the slope of the magnetization (M) with respect to applied magnetic field (H). In the dynamic susceptibility measurement, we measured the two parts of susceptibility, the real (χ') part and imaginary (χ'') part of susceptibility [29)-32)]. Theoretically, the two parts are expressed as follows;

$$\chi'(\omega) = \chi_0 / [1 + (\omega\tau_{eff})^2], \quad (2)$$

$$\chi''(\omega) = \chi_0 \cdot (\omega\tau_{eff}) / [1 + (\omega\tau_{eff})^2], \quad (3)$$

where $\omega = 2\pi f$ is the angular frequency with f the frequency, τ_{eff} the effective relaxation time, and χ_0 is the static susceptibility ($\omega = 0$) described by

$$\chi_0 = (\mu_0 n m^2) / (3k_B T) . \quad (4)$$

with vacuum permeability μ_0, thermal energy k_BT, magnetic moment m, and particle number density n. In this study, the point of interest is the imaginary part of the susceptibility χ'', which can be used to estimate the effective magnetic relaxation time τ_{eff}. At the frequency where χ'' is maximum, the following relation [29)-32)] is true:

$$2\pi f_{peak} \cdot \tau_{eff} = 1, \quad (5)$$

where the f_{peak} is the frequency at χ'' maximum. Therefore, we can calculate τ_{eff} from f_{peak}. The effective relaxation time τ_{eff} is the combination of the two magnetic relaxation processes: Brownian relaxation and Néel relaxation. The Brownian relaxation is due to the physical rotation of nanoparticles, whereas Néel relaxation is from the internal rotation of a magnetic moment of nanoparticles. In general, the faster relaxation mechanism is dominant and τ_{eff} is given by the equation [29)-32)]

$$\tau_{eff} = (\tau_B \cdot \tau_N) / (\tau_B + \tau_N) . \quad (6)$$

The Brownian relaxation time (τ_B) is given by the following equation [26), 29)-32)],

$$\tau_B = [\eta \cdot (d_h)^3] / (2k_B T) . \quad (7)$$

where η is the viscosity of the suspension and d_h is the

hydrodynamic particle diameter. From equation (7), it can be noted that the τ_B is dependent on the hydrodynamic size of the nanoparticle. The Néel relaxation time τ_N is described by [29)-32)]

$$\tau_N = \tau_0 \cdot \exp\left[(\kappa \pi d_c^3) / (6 k_B T)\right] . \quad (8)$$

where κ is the anisotropy constant, d_c is the magnetic core diameter of the nanoparticle, and τ_0 is the intrinsic relaxation time with a typical value of 10^{-9} s [29),31)]. From equation (8), it can be noted that τ_N is dependent on the magnetic core size.

Dynamic susceptibility measurements were made with a magnetic field strength of 10 Oe and frequency range of 10 Hz to 10 kHz. The sample was immersed in different NaCl concentrations (10 mM, 100 mM and 500 mM) before the PPMS measurements. Note that the sample was washed after each measurements and then the same sample was used in the next measurements.

3. Results and Discussion

3.1 Formation of ferrogel

The formation of ferrogel is discussed in this paper to elucidate how the ferrogel have become a porous structure. The actual image of the ferrogel during the gelation time of 1 hour is shown in Fig. 1. The region with a black color is ferrogel, that above the ferrogel is the NH_4OH solution, and that below the ferrogel (colored orange) is the unreacted Fe^{3+}/Fe^{2+}/CH solution. To monitor the height of the ferrogel, photos of specimens were taken with the gelation time. There were 8 photos taken during the 6 hour-observation of the ferrogel. Using an image editor software, the vertical height of the ferrogel was measured in pixels. The height of the container was used as the calibration height to convert the height in pixels to mm. Thus, we are able to accurately estimate the height of the gel via image processing.

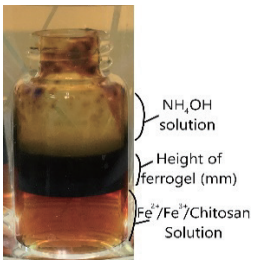

Fig. 1 Actual image of ferrogel. Fe^{2+}/Fe^{3+}/CH solution inside the bottle is submerged in NH_4OH solution. When Fe^{2+}/Fe^{3+}/CH combines with NH_4OH, ferrogel is formed. This image is taken half way thru the synthesis, thus the unreacted Fe^{2+}/Fe^{3+}/CH solution, initially formed ferrogel, and NH_4OH solution are all present. Here, ferrogel membrane separates the two solutions.

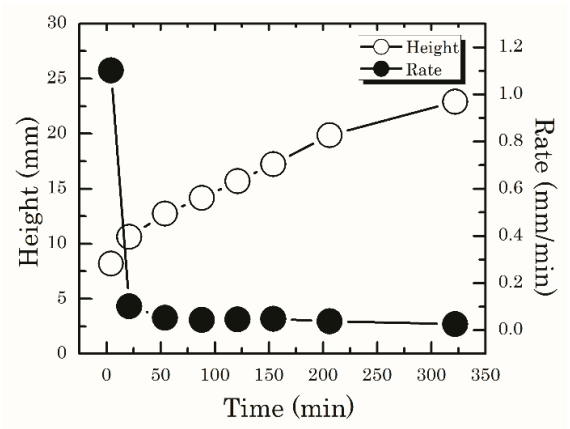

Fig. 2 Measured height of the ferrogel (left y axis, open circles) and the calculated rate of gelation (right y axis, filled circles) are plotted as a function of gelation time.

The calculated ferrogel heights are shown in Fig. 2 (left y axis, open circles). From the figure, it can be observed that the height of the ferrogel monotonically increases with the gelation time. This implies that the ferrogel is porous because it allows the NH_4OH to penetrate into the bottom of the container in order to react and form the additional ferrogel.

The rate of the ferrogel formation is also shown in Fig. 2 (right y axis, filled circles). From the figure, it can be seen that the rate of gelation is decreasing with time. It is also evident from the plots that the calculated initial rate is very high (>1 mm/min) from time = 0 to 30 minutes. Immediately after the initial stage, the rate gradually decreases from time = 30 to 150 min; the rate becomes very slow (<0.1 mm/min) from time = 150 to 350 min. From these data, we can observe that the gel formation rate continuously decreases. This nonlinear gelation behavior suggests that the ferrogels might have different layers within the hydrogel [33)] due to the difference on the rate of diffusion of the OH- from the top to the bottom of the container. Furthermore, this trend is consistent with the idea that as the gel becomes thicker, the diffusion rate naturally becomes slower, leading to the decrease in gel formation rate with time.

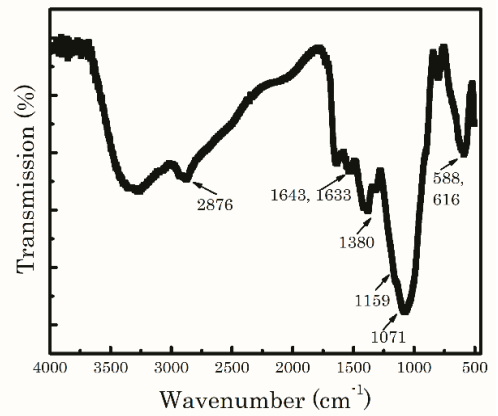

Fig. 3 FTIR spectrum of FeOx-CH.

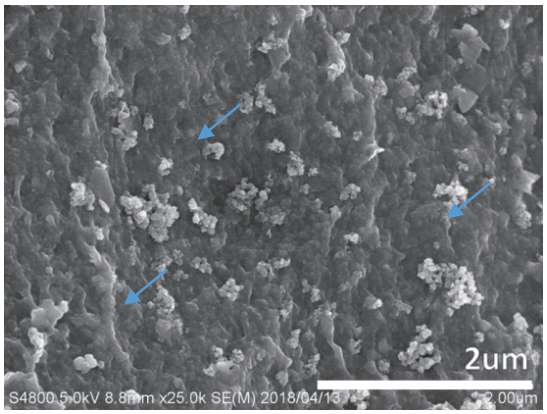

Fig. 4 SEM image of FeOx-CH at 25Kx magnification. Blue arrows point to some of the FeO_x NPs clusters within the ferrogel.

3.2 FTIR and SEM results

Fig. 3 shows the FTIR results of the FeO_x-CH. For CH, the characteristic bands of the asymmetric stretching of the C-H bond appeared around 2876 cm^{-1}. The N-H and C-N vibrations of the amino group present in chitosan is evident at 1633/1643 cm^{-1} and 1380 cm^{-1}, respectively. In addition, the band around 1159/1071 cm^{-1} is from the C-OH stretching of the ester group in chitosan. More importantly, the absorption band at around 600 cm^{-1} is from the Fe-O bond in the FeO_x NPs. From the FTIR data, it can be inferred that high quality CH and FeO_x NPs are present in the composite gels.

An SEM image of FeO_x-CH is shown in Fig. 4. It can be seen from the figure that the NPs (white areas) seem to be clustered and scattered along the striated wall of the CH. The size of the clusters of NPs varies from around 50 nm to 500 nm, with an average of around 150 nm (from 30 sites within the SEM image). This confirms the presence of FeO_x NPs in the composite gel. The SEM image also reveals the irregular/rough porous structure of the CH matrix. In particular, this rough structure increases the surface area of the CH which is desirable to increase sensitivity.

3.3 Swelling ratio at different ionic concentration

The swelling ratio (SR) is plotted as a function of the ionic concentration of solutions in which the FeOx-CH are immersed as shown in Fig. 5. The SR of the FeOx-CH decreases as the ionic concentration of the solution increases. As observed from the figure, it can be concluded that the FeOx-CH is indeed sensitive to changes in the salt concentration change. The degree of swelling of hydrogels depends on the extent on the degree of ionization of functional groups of the hydrogels and the ionic strength of the external solution [23),33)-34)].

One possible explanation on the reduced swelling of the gel, when the surrounding solution of the CH has high ionic strength, is the movement of the water molecule from the lower osmotic pressure inside the CH to the higher osmotic pressure outside the CH.

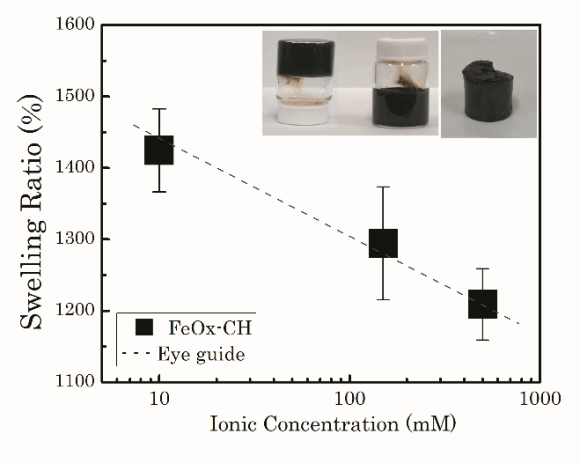

Fig. 5 Swelling ratio of FeO_x-CH with different ionic concentrations. Insets are photographs of actual FeO_x-CH used.

The additional osmotic pressure outside the CH is caused by the presence of cations (Na^+) near the walls of the CH [23)- 34)]. This is also known as the Donnan effect [23)- 34)], wherein, in this case, we consider that CH acts as a semi-permeable membrane. To illustrate this, the schematic of swelling mechanism of FeO_x-CH at different ionic strength is shown in Fig. 6. From the schematic diagram, the black arrows correspond to the amount and the direction of the water flow from outside the gel into the inside the gel. When there is large water flow into the gel, the gel swelling is enhanced, whereas when there is a small water flow into the gel, the gel swelling is reduced. Figure 6 shows that when the NaCl concentration of the surrounding CH is increased, the amount of the water flow inside the CH is small, causing the CH to reduced swelling. In contrast, when the NaCl concentration is decreased, the water flow going to CH is large resulting to an enhance swelling of the CH.

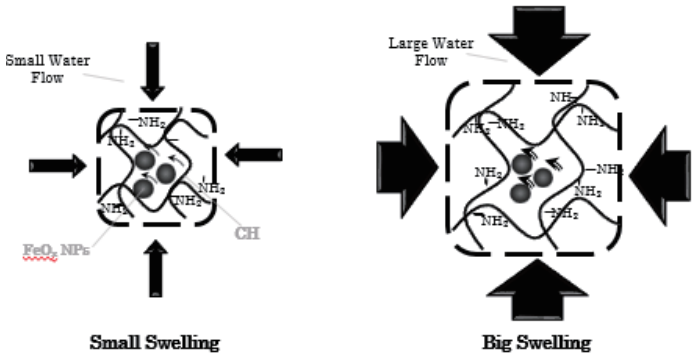

Fig 6. Schematic of FeO_x-CH mechanism when submerged to increasing (left) or decreasing (right) ionic concentration. Black arrows show the amount of water flow inside the gel that causes the reduction and enhancement of the gel swelling. It also illustrates the FeO_x NPs rotation under these two ionic conditions.

3.4 Dynamic susceptibility as a function of ionic strength

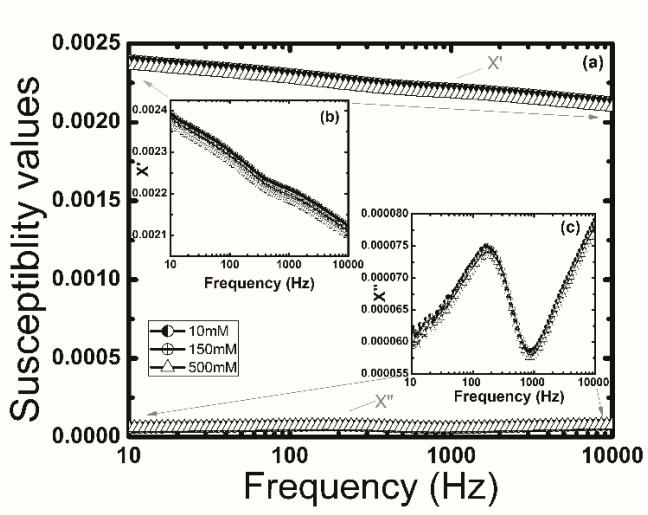

Fig. 7 Dynamic susceptibility of the FeOx-CH (a), the zoomed in real (inset b, top values) and imaginary (inset c, bottom values) parts of the susceptibility at 10mM (◐), 150mM (⊕), and 500mM (△) NaCl concentrations.

As seen in Fig. 7a, the plot of the χ' values are all located in the top part of the plot with high susceptibility values, whereas the plot of the χ'' values are all located at the bottom with low susceptibility values. The plots of the zoomed-in χ'' and χ' values are also shown in Fig. 7b and Fig. 7c, respectively. We can observe from Fig. 7a that the χ'' values are very small compared to χ' values at lower frequencies ($\chi'' / \chi' \approx 0.026$), hence, it is expected that the area inside M-H hysteresis curve at these frequencies would be proportionally small (almost no hysteresis in M-H curve is expected) which is a characteristic of superparamagnetism. Further, as can be seen in the Fig. 7b (inset), it is evident that χ' is decreasing as the frequency increases. This decreasing behavior is a typical signature of the real part of the susceptibility for superparamagnetic nanoparticles [35] as the frequency crosses the f_{peak} of the sample.

We can see in Fig. 7b (inset) that χ' slightly decreases (shift downwards) with the increase of the ionic concentration. This downward shift seems to be related to the corresponding change in χ'' with ionic concentration. This is elucidated in the next paragraph. Note also that the order of magnitude of the χ' values does not change, which suggests that the total moment of the ferrogel sample did not change between measurement, which is expected and a sign of good experimental reproducibility and reliability of the sample.

For all the ionic conditions, it can be observed in Fig. 7c (inset) that there is a clear χ'' peak at around 200 Hz, corresponding to an effective relaxation time of τ_{eff} of around 0.8 msec. Also, the χ'' values are again increasing at >> 1 kHz which could correspond to another high frequency peak. Moreover, the χ'' plot shown in Fig. 7c (inset) are shifted to lower frequency with the increase of the ionic concentration. This low-frequency shift of the χ'' would also cause a corresponding low-frequency shift in the χ'. However, since there is no peak in the χ', this low-frequency shift may appear as a downward shift, which we see in the Fig. 7b results.

Shown in the inset of Fig. 8 is the plot of the zoomed-in normalized χ'' from the data in Fig. 7c. In the normalization of χ'', the minimum χ'' value (found at the low frequency end) is set to 0, whereas the local maximum χ'' peak value (found around 200 Hz) is set to 1. Note that at the low frequency end, the value of χ'' is very much smaller than that of χ' values and practically is zero. Also, in Fig. 8 inset, the normalized χ'' values are vertically separated for visual clarity of the shift in f_{peak}. It can be seen that the position of the maximum χ'' shift to lower frequency as the ionic strength increases. A plot of f_{peak} for different ionic strength are shown in Fig. 8. These f_{peak} values are extracted from the fitted Gaussian function of the data from the inset of Fig. 8. It is evident from Fig. 8 that there is a shift in the χ'' peak position to lower frequencies from ~193 Hz to ~182 Hz upon increase of the ionic concentration of the solution from 10 mM to 500 mM. We also note the strong correlation between the SR in Fig. 5 to f_{peak} in Fig. 8, which clearly suggests that the reduced swelling of the ferrogel is related to the shift in f_{peak}.

As previously mentioned in Section 2.3, the point of interest in this study is in the magnetic relaxation (τ_{eff}) of the FeO_x NPs in the ferrogel, we can estimate the τ_{eff} from f_{peak} by applying Eq. (5). Here, we find τ_{eff} was increased from 0.874 msec to 0.825 msec as the ionic strength increases from 10 mM to 500 mM.

In order to explain these results, we need to determine the dominant magnetic relaxation mechanism in the present sample. We note that the Néel relaxation time τ_N is not affected by changes in ionic concentration or reduced swelling of the ferrogel, whereas the Brownian relaxation time can be affected. When the ferrogel reduced swelling, it likely becomes more difficult for the FeO_x NPs to rotate, especially if we consider clustered NPs as suggested by the SEM imaging results. This increased difficulty of rotation effectively suppresses the Brownian relaxation of the NPs. This can be interpreted as an increase in the effective viscosity of the surrounding gel. Therefore, the fact that a shift f_{peak} was observed strongly suggests that in the sample in the current study Brownian relaxation is dominant, as Néel relaxation alone would not explain the f_{peak}.

Note that although the reduced swelling of the gel also changes the spacing between NPs which can also affect τ_{eff}, the trend, however, is opposite. If we consider the spacing between NPs, the reduced swelling of the gel would yield to the decrease in spacing between NPs, which would enhance the dipolar interaction, which should in-turn decrease τ_{eff} [39)-40)]. That is when high density (small spacing) of NPs are present, relaxation is

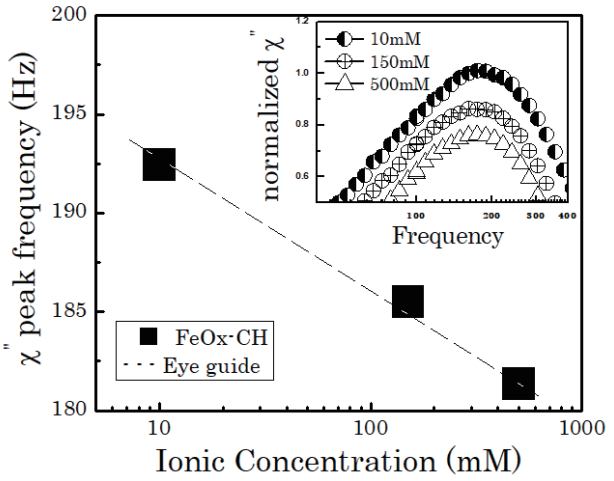

Fig 8. Peak frequency f_{peak} of χ'' as function of ionic concentration of the FeO_x-CH. Inset: plot of the normalized χ'' as function of frequency at different ionic concentrations, zoomed-in and vertically separated for visual clarity of the position of f_{peak}.

enhanced. We note that this is in fact opposite the results of the present study, and is therefore unlikely. Moreover, since the NPs are arranged in clusters, the dipolar interaction between individual particles is already present even without changing the ionic concentration. Hence, changing the interparticle spacing due the ionic concentration (and reduced swelling of the gel) is not expected to increase the dipolar interaction significantly.

Furthermore, if we consider the only the effect of ionic concentration to NPs (the case without a CH gel matrix), we expect that an increase in the ionic concentration leads to the surface charges in the NPs, which would prevent aggregation as well as increases inter-particle spacing [41)-43)]. Again, this, however, is opposite the results of the present study, where the presence and reduction of swelling of the CH gel causes the formation of clusters and the spacing between NPs to decrease. Therefore, the possibility that the ionic concentration (chemical stimuli) is affecting the magnetic properties NPs directly is unlikely, and that it is more probable that the ionic concentration directly interacts with the CH gel and CH gel in-turn affects the magnetic property of the NPs by suppressing the Brownian relaxation.

After these considerations, we therefore infer that for the sample in the present study, Brownian relaxation is dominant ($\tau_{eff} \approx \tau_B$ [35)-37)], and $\tau_B << \tau_N$). This allows us to estimate the hydrodynamic size d_h. Using Eq. (7), we estimated d_h of around 130 nm for η = 1 mPa.s [44)]. We note that this value agrees well with the clustered NPs size showed in our SEM results. Whereas, we attribute the high frequency χ'' peak (at >> 1 k Hz in Fig. 7c-inset) to the non-clustered NPs in the ferrogel. Assuming that the high frequency peak is comparable to that of a similar sample, it is expected to be in the order of 10 kHz, which corresponds to a $\tau_B \approx 16$ μsec and $d_h \approx 34$ nm. Note that the NPs d_h and d_c are of the same order of magnitude, which is expected. Furthermore, this also allows us to estimate the minimum possible magnetic core size of the NPs. Since Brownian relaxation is dominant, $\tau_N >> \tau_B \approx$ 0.80 msec. Assuming τ_N is in the order of 8 msec, we estimate a magnetic core size of around 18.41 nm for κ = 2 x 10^4 Joule·m^{-3} [45)-46)]. This again fits well with the SEM results, since the magnetic core size should be smaller than the cluster size. Note that this is just the lower bound for the magnetic core size of the NPs.

Similar to the analysis done in the previous study [6)], it is reasonable to assume that the Néel relaxation time remains the same even if the ionic concentration changes. Therefore, the presence of the experimentally observed frequency shift suggests that Brownian relaxation is dominant in the present specimens. Ignoring the contribution of Néel relaxation (i.e. $2\pi f_{peak} \approx 1/\tau_B$) [36)-38)], we can relate the change in the effective viscosity $\Delta\eta$ to the experimentally observed shift in peak frequency, Δf_{peak}, due to ionic concentration change. This relation is analytically written as

$$\Delta f_{peak} \approx (2\, k_B T \Delta\eta) / (\pi d_h^3 \eta) = (\Delta\eta / \eta) \times \tau_B, \qquad (9)$$

where the parameter $\Delta\eta/\eta$ is the fractional (or percent) change of the viscosity. Equation (9) is derived by taking the derivative of the reciprocal of Eq. (5) with respect to η. From the experimentally measured frequency shift of $\Delta f_{peak} \approx 11$ Hz due to ionic concentration change, a change in the viscosity $\Delta\eta/\eta \approx 6.13\%$ is estimated. We estimate that the viscosity change of the surrounding medium is increased from 1 mPa.s to 1.0613 mPa.s when the ionic concentration is increased. This is smaller compared to our previous result on the effect of pH. This signifies that the ferrogel is more sensitive to pH than to ionic strength values used in the experiments.

4. Conclusion

In the present study, we experimentally demonstrated the use of CH ionic strength sensitivity to affect the magnetic relaxation properties of FeO_x NPs. The observed shift to lower frequency of the χ'' peak is due to the reduced swelling of the hydrogel that suppresses the Brownian relaxation. The change of effective viscosity is also estimated by analytical calculations. The results in this study is a promising demonstration of magnetic sensing of chemical stimuli that may be useful for future bio-sensing applications.

Acknowledgements This work was partly supported by the following foundations: Tokyo Ohka Foundation, Kato Foundation and Murata Science Foundation.

References

1) J.S. Gonzalez, P. Nicolás, M.L. Ferreira, M. Avena, V.L. Lassalle, V.A. Alvarez: *POLYM INT.*, **63**, 258 (2012).
2) S. Kennedy, C. Roco, A. Déléris, P. Spoerri, C. Cezar, J. Weaver, H. Vandenburgh, and D. Mooney: *Biomaterials*, **161**, 179 (2018).

3) Y. Lu, W. He, C. Cao, H. Guo, Y. Zhang, Q. Li, Z. Shao, Y. Cui, and X. Zhang: *Sci Rep.*, **4**, 5792 (2014).
4) X. Zhao, J. Kim, C.A. Cezar, N. Huebsch, K. Lee, K. Bouhadir, and D.J. Mooney: *Proc. Natl. Acad. Sci.*, **108**, 67 (2011).
5) N.S. Satarkar, W. Zhang, R.E. Eitel, and J.Z. Hilt: *Lab Chip*, **9**, 1773 (2009).
6) M.E. Villamin, and Y. Kitamoto: *IEEE Trans. Magn.*, **55**, 1 (2019).
7) Koetting, M. C., Peters, J. T., Steichen, S. D., & Peppas, N. A.: *Mater. Sci. Eng. R Rep.*, **93**, 1 (2015).
8) Ma, C., Shi, Y., Pena, D. A., Peng, L., & Yu, G.: *Angew. Chem.*, **127**, 7484 (2015).
9) Dragan, E. S., & Cocarta, A. I.: *ACS Appl. Mater. Interfaces*, **8**, 12018 (2016).
10) Wei, M., Gao, Y., Li, X., & Serpe, M. J.: *Polym. Chem.*, **8**, 127 (2017).
11) M. Bally, M. Halter, J. Vörös, and H.M. Grandin: *Surf. Interface Anal.* **38**, 1442 (2006).
12) A. Syahir, K. Usui, K.Y. Tomizaki, K. Kajikawa, and H. Mihara: *Microarrays (Basel)*, **4**, 228 (2015).
13) H.J. Hong, W.S. Koom, and W.G. Koh: *Sens.*, **17**, 1293 (2017).
14) M. Rizwan, R. Yahya, A. Hassan, M. Yar, A.D. Azzahari, V. Selvanathan, F. Sonsudin, and C.N. Abouloula: *Polymers*, **9**, 137 (2017).
15) H.S. Lee, M.Q. Yee, Y.Y. Eckmann, N.J. Hickok, D.M. Eckmann, and R.J. Composto: *J Mater Chem*, **22**, 19605 (2012).
16) S.K. Samal, M. Dash, P. Dubruel, and S. V. Vlierberghe: Smart polymers and their applications, Chapter 8, p. 237-270 (Elsevier, 2014).
17) J. Cho, M.C. Heuzey, A. Bégin, and P.J. Carreau: *J Food Eng.*, **74**, 500 (2006).
18) S. Kunjachan, S. Jose, and T. Lammers: *Asian J. Pharm.,* **4**, 2 (2014).
19) F. Lai, H. Li, and R. Luo: *Int J Solids Struct.*, **47**, 3141 (2010).
20) X. Zhang, H. Niu, Y. Pan, Y. Shi, and Y. Cai: *Anal. Chem.*, **82**, 2363 (2010).
21) F.M. Goycoolea, M.E. Fernández - Valle, I. Aranaz, and A. Heras: *Macromol Chem Phys.,* **212**, 887 (2011).
22) S. Dimida, C. Demitri, V.M. Benedictis, F. Scalera, F. Gervaso, and A. Sannino: *J Appl Polym Sci.* **132**, (2015).
23) G.R. Deen, and X.J. Loh: *Gels*, **4**, 13 (2018).
24) W. Zhang, X. Li, R. Zou, H. Wu, H. Shi, S. Yu, and Y. Liu: *Sci. Rep.*, **5**, 11129 (2015).
25) W.S. Peternele, V.M. Fuentes, M.L. Fascineli, J.R.D. Silva, R.C. Silva, C.M. Lucci, and R.B.D. Azevedo: *J NANOMATER*, **2014**, 94 (2014).
26) A.G. Kolhatkar, A.C. Jamison, D. Litvinov, R.C. Willson, and T.R. Lee: *Int. J. Mol. Sci.,* **14**, 15977 (2013).
27) Kim, S. J., Park, S. J., & Kim, S. I. (2003). *React. Funct. Polym.,* **55**, 53 (2003).
28) Fan, L., Yang, H., Yang, J., Peng, M., & Hu, J.: *CARBOHYD POLYM*, **146**, 427 (2016).
29) J. Dieckhoff, D. Eberbeck, M. Schilling and F. Ludwig: *J. Appl. Phys.*, **119**, 043903 (2016).
30) F. Ludwig, C. Balceris, C. Jonasson, and C. Johansson: *IEEE Trans. Magn.,* **53**, 1 (2017).
31) S. Bogren, A. Fornara, F. Ludwig, M. del Puerto Morales, U. Steinhoff, M.F. Hansen, O. Kazakova, and C. Johansson: *Int J Mol Sci.*, **16**, 20308 (2015).
32) V. Singh, V. Banerjee, M. and Sharma: *J. Phys. D.*, **42**, 245006 (2009)
33) J. Nie, W. Lu, J. Ma, L. Yang, Z. Wang, A. Qin, and Q Hu: Sci. Rep., **5**, 7635 (2015).
34) J. Ricka, T. Tanaka: 1984. *Macromolecules*, **17**, 2916 (1984).
35)Fannin, P. C., Scaife, B. K. P., & Charles, W.: *J. Phys. E: Sci. Instrum.,* **19**, 238 (1986).
36) Wu, K., Liu, J., Wang, Y., Ye, C., Feng, Y., & Wang, J. P.: *Appl. Phys. Lett.*, **107**, 5 (2015).
37) Wu, K., Ye, C., Liu, J., Wang, Y., Feng, Y., & Wang, J. P.: IEEE Trans. Magn., **52**, 1 (2016).
38) Tu, L., Wu, K., Klein, T., & Wang, J. P.: *J. Phys. D.*, **47**, (2014).
39)Orozco-Henao, J. M., Coral, D. F., Muraca, D., Moscoso-Londoño, O., Mendoza Zélis, P., Fernandez van Raap, M. B., & Knobel, M.: *J. Phys. Chem. C*, **120**, 12796 (2016).
40)Allia, Paolo, Marco Coisson, Paola Tiberto, Franco Vinai, Marcelo Knobel, M. A. Novak, and W. C. Nunes.: *Phys. Rev. B*, **64**, 144420 (2001).
41)Mirshahghassemi, S., Cai, B., & Lead, J. R.: *Environmental Science: Nano*, **3**, 780 (2016).
42)Nesztor, D., Bali, K., Tóth, I. Y., Szekeres, M., & Tombácz, E.: J. *Magn. Magn. Mater*, **380**, 144 (2015).
43)Tombácz, E., Farkas, K., Földesi, I., Szekeres, M., Illés, E., Tóth, I. Y., Nesztor, D. & Szabó, T.: *Interface focus*, **6**, (2016).
44) Jia, D., Hamilton, J., Zaman, L. M., & Goonewardene, A.: *Am. J. Phys.,* **75**, 111 (2007).
45) Nayek, C., Manna, K., Imam, A. A., Alqasrawi, A. Y., & Obaidat, I. M.: *In IOP Conference Series: Materials Science and Engineering*, **305**, (012012). IOP Publishing. (2018).
46) Demortiere, A., Panissod, P., Pichon, B. P., Pourroy, G., Guillon, D., Donnio, B., & Begin-Colin, S.: *Nanoscale*, **3**, 225 (2011).

Received Oct. 16, 2018; Revised Dec. 27, 2018; Accepted Feb. 15, 2019